UCRHEP-T428
MSUHEP-061208

Resummation Effects in the Search of SM Higgs Boson at Hadron Colliders

Qing-Hong Cao*
Department of Physics and Astronomy,
University of California at Riverside, Riverside, CA 92521

Chuan-Ren Chen†
Department of Physics and Astronomy,
Michigan State University, E. Lansing, MI 48824

Abstract

We examine the soft-gluon resummation effects, including the exact spin correlations among the final state particles, in the search of the Standard Model Higgs boson, via the process $gg \to H \to WW/ZZ \to 4\,\text{leptons}$, at the Tevatron and the LHC. A comparison between the resummation and the Next-to-Leading order (NLO) calculation is performed after imposing various kinematics cuts suggested in the literature for the Higgs boson search. For the $H \to ZZ$ mode, the resummation effects increase the acceptance of the signal events by about 25%, as compared to the NLO prediction, and dramatically alter various kinematics distributions of the final state leptons. For the $H \to WW$ mode, the acceptance rates of the signal events predicted by the resummation and NLO calculations are almost the same, but some of the predicted kinematical distributions are quite different. Thus, to precisely determine the properties of the Higgs boson at hadron colliders, the soft-gluon resummation effects have to be taken into account.

*Electronic address: qcao@ucr.edu
†Electronic address: crchen@pa.msu.edu

I. INTRODUCTION

Although Standard Model (SM) explains successfully all current high energy physics experimental data, the mechanism of electoweak spontaneous symmetry breaking, arising from the Higgs mechanism, has not yet been tested directly. Therefore, searching for the Higgs boson (H) is one of the most important tasks at the current and future high energy physics experiments. The negative result of direct search at the LEP2, via the Higgsstrahlung process $e^+e^- \to ZH$, poses a lower bound of 114.1 GeV on the SM Higgs boson mass (M_H) [1]. On the other hand, global fits to electroweak observables prefer $M_H \lesssim 200\,\text{GeV}$ at the 95% confidence level [2], while the triviality arguments put an upper bound $\sim 1\,\text{TeV}$ [3].

There is currently an active experimental program at the Tevatron to directly search for the Higgs boson. The Large Hadron Collider (LHC) at CERN, scheduled to operate in late 2007, is expected to establish the existence of Higgs boson if the SM is truly realized in Nature. At the LHC, the SM Higgs boson is mainly produced through gluon-gluon fusion process induced by a heavy (top) quark loop. Once being produced, it will decay into a fermion pair or vector boson pair. The strategy of searching for the Higgs boson depends on how it decays and how large the decay branching ratio is. If the Higgs boson is lighter than 130 GeV, it mainly decays into a bottom quark pair ($b\bar{b}$). Unfortunately, it is very difficult to search for the Higgs boson in this mode due to the extremely large Quantum Chromodynamics (QCD) background at the LHC. However, the $H \to \gamma\gamma$ mode can be used to detect a Higgs boson with the mass below 150 GeV [4, 5] though the decay branching ratio of this mode is quite small, $\sim O(10^{-3})$. If the Higgs boson mass (M_H) is in the region of 130 GeV to $2M_Z$ (M_Z being the mass of Z boson), the $H \to ZZ^*$ mode is very useful because of its clean collider signature of four isolated charged leptons. The $H \to WW^{(*)}$ mode is also important in this mass region because of its large decay branching ratio. When $M_H > 2M_Z$, the decay mode $H \to ZZ \to \ell^+\ell^-\ell'^+\ell'^-$ is considered as the "gold-plated" mode which is the most reliable way to detect the Higgs boson up to $M_H \sim 600\,\text{GeV}$ because the backgrounds are known rather precisely and the two on-shell Z bosons could be reconstructed experimentally. For $M_H > 600\,\text{GeV}$, one can detect the $H \to ZZ \to \ell^+\ell^-\nu\bar{\nu}$ decay channel in which the signal appears as a Jacobian peak in the missing transverse energy spectrum.

The discovery of the Higgs boson relies on how well we understand the signals and its backgrounds, because one needs to impose optimal kinematics cuts to suppress the huge

backgrounds and enhance the signal to background ratio (S/B). Many works have been done in the literature to calculate the higher order QCD corrections to the dominant production process of the Higgs boson $gg \to H$ [6, 7, 8, 9, 10, 11, 12, 13, 14, 15, 16, 17, 18]. In addition to determine the inclusive production rate of the Higgs boson, an accurate prediction of kinematics of the Higgs boson is very essential for the Higgs boson search. However, a fix order calculation cannot reliably predict the transverse momentum (Q_T) distribution of Higgs boson for the low Q_T region where the bulk events accumulate. This is because of large corrections of the form $\ln(Q^2/Q_T^2)$ due to non-complete cancellations of soft and collinear singularities between virtual and real contributions, where Q is the invariant mass of the Higgs boson. Therefore, one needs to take into account the effects of the initial state multiple soft-gluon emissions in order to make a reliable prediction on the kinematic distributions of the Higgs boson. One approach to achieve this is to include parton showering [19] which resums the universal leading logs in Monte Carlo event generators, e.g. HERWIG [20] and PYTHIA [21], which are commonly used by experimentalists. The showering process just depends on the initial state parton and the scale of the hard process being considered. The advantage is that it could be incorporated into various physics processes. Recently, an approach to match NLO matrix element calculation and parton showing Monte Carlo generators, MC@NLO [22, 23], has been proposed. Another approach is to include correctly the soft-gluon effects is to calculate an analytical result by using the Collins-Soper-Sterman (CSS) resummation formalism [24, 25, 26, 27] to resum these large logarithmic corrections to all order in α_s. However, in practice the power of logarithms included in Sudakov exponent depends on which level the fixed order calculation has been performed [28, 29, 30, 31, 32]. It is very interesting to compare the predictions between parton showering and resummation calculation and detailed comparisons have been presented in Ref. [28, 33, 34, 35, 36] which concluded that all of the distributions are basically consistent with each other, except PYTHIA in the small Q_T region and HERWIG in the large Q_T region.

In addition, the spin correlation among the Higgs decay products has been proved to be crucial to suppress the backgrounds [37, 38]. Hence, an accurate theoretical prediction, which incorporates the initial state soft-gluon resummation effects and the spin correlations among the Higgs decay products, is needed. In this paper, we present such a calculation and study the soft-gluon resummation (RES) effects on various kinematics distributions of final state particles. Furthermore, we examine the impact of the RES effects on the

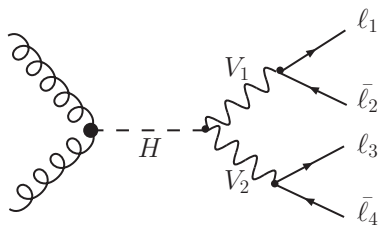

Figure 1: Tree level Feynman diagram of process $gg \to H \to V_1(\to \ell_1\bar{\ell}_2)V_2(\to \ell_3\bar{\ell}_4)$.

acceptance rate of the signal events with various kinematics cuts (which were suggested in the literature [37, 39] for Higgs search) and compare them with the leading order (LO) and NLO predictions [1].

The paper is organized as follows. In Sec. II, we present our analytical formalism of the CSS resummation. In Sec. III, we present the inclusive cross section of the signal process for several benchmark masses of the Higgs boson. In Sec. IV, we study the process $gg \to H \to WW^{(*)} \to \ell^+\ell'^-\nu_\ell\bar{\nu}_{\ell'}$ for $M_H = 140\,\text{GeV}$ at the Fermilab Tevatron and for $M_H = 170\,\text{GeV}$ at the LHC. In Sec. V, we examine the process $gg \to H \to ZZ^{(*)} \to \ell^+\ell^-\ell'^+\ell'^-$ for $M_H = 140\,\text{GeV}$ and $200\,\text{GeV}$, respectively, and the process $gg \to H \to ZZ \to \ell^+\ell^-\nu\bar{\nu}$ for $M_H = 600\,\text{GeV}$, at the LHC. Our conclusions are given in Sec. VI.

II. TRANSVERSE MOMENTUM RESUMMATION FORMALISM

At the hadron colliders, the SM Higgs boson is mainly produced via gluon-gluon fusion process through a heavy quark triangle loop diagram, cf. Fig 1, in which the effect of the triangle loop is replaced by the effective ggH coupling (denoted as the bold dot). Taking advantage of the narrow width of the Higgs boson, we can factorize the Higgs boson production from its sequential decay. The resummation formula was already presented in Ref.

[1] The NLO Quantum Electrodynamics (QED) and electroweak (EW) corrections to the Higgs decay process $H \to WW/ZZ \to 4\ell$ were calculated in Ref. [40] and Ref. [41], respectively. Recently, the NLO QCD correction to the Higgs boson decays $H \to WW/ZZ \to 4q$ with hadronic four-fermion final states was calculated in Ref. [42]. Since the higher order corrections for Higgs production are dominated by the initial state soft-gluon resummation effects, we focus our attention on the RES effects in this work. It is worth mentioning that the NLO QED corrections to the Higgs boson decay $H \to WW/ZZ \to 4\ell$ have been implemented in ResBos [43] program, and the phenomenological study of the combined RES effects and the QED correction will be presented elsewhere.

[28]. Here, we list some of the relevant formulas as follows, for completeness:

$$\begin{aligned}
&\frac{d\sigma(h_1h_2 \to H(\to VV \to \ell_1\ell_2\ell_3\ell_4)X)}{dQ^2dQ_T^2dyd\phi_H d\Pi_4} \\
&= \sigma_0(gg \to H)\frac{Q^2}{S}\frac{Q^2\Gamma_H/m_H}{(Q^2-m_H^2)^2+(Q^2\Gamma_H/m_H)^2} \\
&\times \left|\mathcal{M}(H \to V_1V_2 \to \ell_1\ell_2\ell_3\ell_4)\right|^2 \\
&\times \left\{\frac{1}{(2\pi)^2}\int d^2b\, e^{iQ_T\cdot b}\tilde{W}_{gg}(b_*,Q,x_1,x_2,C_{1,2,3})\tilde{W}_{gg}^{NP}(b,Q,x_1,x_2) + Y(Q_T,Q,x_1,x_2,C_4)\right\} \quad (1)
\end{aligned}$$

where Q, Q_T, y, and ϕ_H are the invariant mass, transverse momentum, rapidity, and azimuthal angle of the Higgs boson, respectively, defined in the lab frame, and $d\Pi_4$ represents the four-body phase space of the Higgs boson decay, defined in the Collin-Soper frame [44]. In Eq. (1), $|\mathcal{M}(\cdots)|^2$ denotes the matrix element square of the Higgs boson decay and reads as

$$\begin{aligned}
&\left|\mathcal{M}(H \to V_1V_2 \to \ell_1\ell_2\ell_3\ell_4)\right|^2 \\
&= 16\sqrt{2}G_F^3m_V^8\frac{1}{(q_1^2-m_V^2)^2+m_V^2\Gamma_V^2}\frac{1}{(q_2^2-m_V^2)^2+m_V^2\Gamma_V^2} \\
&\times \left[C_+(p_1\cdot p_3)(p_2\cdot p_4)+C_-(p_1\cdot p_4)(p_2\cdot p_3)\right],
\end{aligned}$$

where m_V is the vector boson mass, $q_i(p_i)$ denotes the momentum[2] of the vector boson V_i (the lepton ℓ_i), and G_F is the Fermi coupling constant. Here,

$$C_\pm = \left(a_{12}^2+b_{12}^2\right)\left(a_{34}^2+b_{34}^2\right) \pm 4a_{12}b_{12}a_{34}b_{34},$$

where a_{12} and b_{12} respectively denote the vector and axial vector components of the $V\ell_1\ell_2$ coupling, while a_{34} and b_{34} are the ones for $V\ell_3\ell_4$. For the W boson, $m_V = m_W$, and

$$a = b = \sqrt{2},$$

while for the Z boson, $m_V = m_Z$, and

$$\begin{aligned}
a &= 4\sin\theta_W^2 - 1, \;\; b = -1 \;\text{ for }\; Z \to \ell^+\ell^-, \\
a &= 1,\, b = 1 \quad \text{for }\; Z \to \nu\bar{\nu},
\end{aligned}$$

[2] The direction of momentum p_i is defined to be outgoing from the mother particle.

where θ_W is the weak mixing angle. In Eq. (1), the function $\tilde{W}_{gg}$ sums over the soft gluon contributions that grow as $Q_T^{-2} \times [1 \text{ or } \ln(Q_T^2/Q^2)]$ to all order in α_S, which contains the singular part as $Q_T \to 0$. The contribution which is less singular than those included in $\tilde{W}_{gg}$ is calculated order-by-order in α_S and is included in the Y term. Therefore, we can obtain the NLO results by expending the above resummation formula, i.e. Eq. (1), to the α_S^3 order. More details can be found in Ref. [43]. In our calculation, σ_0 includes the complete LO contribution with finite quark mass effects [45, 46, 47, 48]. It has been shown [9] that this prescription approximates well the exact NLO inclusive Higgs production rate.

For the numerical evaluation, we chose the following set of SM input parameters [49]:

$$\begin{aligned} G_F = 1.16637 \times 10^{-5}\text{GeV}^{-2}, \quad & \alpha = 1/137.0359895, \\ m_Z = 91.1875\,\text{GeV}, \quad & \alpha_s(m_Z) = 0.1186, \\ m_e = 0.5109997\,\text{MeV}, \quad & m_\mu = 0.105658389\,\text{GeV}. \end{aligned}$$

Following Ref. [50], we derive the W boson mass as $m_W = 80.385\,\text{GeV}$. Thus, the square of the weak gauge coupling is $g^2 = 4\sqrt{2}m_W^2 G_F$. Including the $\mathcal{O}(\alpha_s)$ QCD corrections to $W \to q\bar{q}'$, we obtain the W boson width as $\Gamma_W = 2.093\,\text{GeV}$ and the decay branching ratio of $\text{Br}(W \to \ell\nu) = 0.108$ [51]. In order to include the effects of the higher order electroweak corrections, we also adapt the effective Born approximation in the calculation of the $H \to ZZ \to 4\,\text{leptons}$ mode by replacing the $\sin^2\theta_W$ in the $Z\ell\ell$ coupling by the effective $\sin^2\theta_W^{eff} = 0.2314$, calculated at the m_Z scale.

III. INCLUSIVE CROSS SECTIONS

For the mass of the Higgs boson being within the intermediate mass range, it will principally decay into two vector bosons which sequentially decay into either lepton or quark pairs. Leptons are the objects which can be easily identified in the final state, so the di-lepton decay mode is regarded as the "golden channel" due to its clean signature and well-known background. The drawback is that the di-lepton mode suffers from the small decay branching ratio for the vector boson decay ($V \to \ell\bar{\ell}$). For example, the branching ratio of $Z \to \ell^+\ell^-$ is only about 3.4%. Due to the huge QCD backgrounds, the purely hadronic decay modes are not as useful for detecting the Higgs boson.

In this paper, we focus on the purely leptonic decays of the vector bosons in the $H \to$

Table I: Inclusive cross sections of $gg \to H \to VV \to 4\ell$ at the Tevatron Run 2 and the LHC in the unit of fb, i.e. $\sigma(gg \to H) \times Br(H \to VV) \times Br(V \to \ell_1\ell_2) \times Br(V \to \ell_3\ell_4)$ for various Higgs boson masses. Here, ℓ and ℓ' denote either e or μ.

	$WW^{(*)} \to \ell^+\ell'^-\nu_\ell\bar{\nu}_{\ell'}$		$ZZ^{(*)} \to \ell^+\ell^-\ell'^+\ell'^-$		$ZZ \to \ell^+\ell^-\nu\bar{\nu}(=\sum_{i=e,\mu,\tau}\nu_i\bar{\nu}_i)$
M_H	140 GeV	170 GeV	140 GeV	200 GeV	600 GeV
	Tevatron	LHC	LHC	LHC	LHC
RES	13.1	891.1	11.0	17.7	6.3
NLO	11.5	848.9	10.5	16.4	5.6
LO	4.0	405.3	5.1	8.0	2.4

$WW^{(*)}$ and $H \to ZZ^{(*)}$ modes. To cover the intermediate mass range, we consider the following benchmark cases: (i) $H \to WW^{(*)} \to \ell^+\ell'^-\nu_\ell\bar{\nu}_{\ell'}$ ($\ell, \ell' = e$ or μ) for $M_H = 140\,\text{GeV}$ at the Femilab Tevatron Run 2 (a 1.96 TeV $p\bar{p}$ collider), and for $M_H = 170\,\text{GeV}$ at the LHC (a 14 TeV pp collider); (ii) $H \to ZZ^{(*)} \to \ell^+\ell^-\ell'^+\ell'^-$ ($\ell, \ell' = e$ or μ) for $M_H = 140$ and $200\,\text{GeV}$ at the LHC; (iii) $H \to ZZ \to \ell^+\ell^-\nu\bar{\nu}$ for $M_H = 600\,\text{GeV}$ at the LHC, where $\ell = e$ or μ, and $\nu = \nu_e$, ν_μ or ν_τ. All the numerical results are calculated by using ResBos [43]. We adapt CTEQ6.1L parton distribution function in the LO calculation and CTEQ6.1M parton distribution function [52] in the NLO and RES calculations. The renormalization scale (μ_R) and factorization scale (μ_F) are chosen to be the Higgs boson mass in our calculations, i.e. $\mu_R = \mu_F = M_H$.

The inclusive cross sections for those benchmark masses of the Higgs boson are summarized in Table I where different searching channels are considered. For comparison, we show the Q_T distributions calculated by using the RES and NLO calculations in Fig. 3(a). The RES calculation is similar to that presented in Ref. [28, 29] with the known A and B [53, 54, 55, 56, 57], but with $A_g^{(3)}$ included, where [58]

$$A_g^{(3)} = \frac{C_A C_F N_f}{2}(\zeta(3) - \frac{55}{48}) - \frac{C_A N_f^2}{108} + C_A^3(\frac{11\zeta(3)}{24} + \frac{11\pi^4}{720} - \frac{67\pi^2}{216} + \frac{245}{96}) + C_A^2 N_f(-\frac{7\zeta(3)}{12} + \frac{5\pi^2}{108} - \frac{209}{432}), \quad (2)$$

where $C_A = 3$, $C_F = 4/3$, $N_f = 5$ and the Riemann constant $\zeta(3) = 1.202...$. We also use the modified parton momentum fractions x_1 and x_2 to take into account the kinematic corrections due to the emitted soft gluons [28], with $x_1 = m_T e^y/\sqrt{S}$ and $x_2 = m_T e^{-y}/\sqrt{S}$,

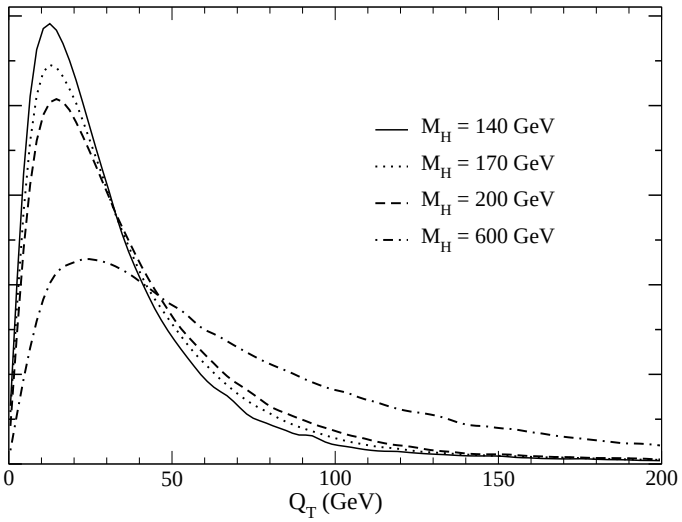

Figure 2: Normalized distributions of transverse momentum of Higgs boson predicted by RES calculation at the LHC.

where $m_T = \sqrt{Q_T^2 + Q^2}$ and $\sqrt{S}$ is the center-of-mass energy of the hadron collider. We also adopt the matching procedure described in the Ref. [43] and the non-perturbation contribution $\tilde{W}^{NP}$ of BLNY form in the Ref. [59]. In Fig. 2, we show the transverse momentum distributions of Higgs boson predicted by RES calculation at the LHC. As we see that the peak position is shifted to larger Q_T region and the shape becomes broader when the mass of Higgs becomes heavier.

It is clear that the prediction of NLO calculation blows up in the $Q_T \to 0$ region and the RES effects have to be included to make a reliable prediction on event shape distributions. In the NLO calculation, it is ambiguous to treat the singularity of the Q_T distribution near $Q_T = 0$, see the dashed curve in Fig. 3(a). Before presenting our numerical results, we shall explain how we deal with the singularity in the NLO calculation when $Q_T \sim 0$. In ResBos, we divide the Q_T phase space with a separation scale Q_T^{sep}. We calculate the Q_T singular part of real emission and virtual correction diagrams analytically and integrate the sum of these two parts up to Q_T^{sep}. By this procedure, it yields a finite NLO cross section, for integrating Q_T from 0 up to Q_T^{sep}, which is put into the $Q_T = 0$ bin of the NLO Q_T distribution (for bin width larger than Q_T^{sep}). Since the separation scale Q_T^{sep} is introduced in the theoretical calculation for technical reasons only and is not a physical observable, the sum of both contributions from $Q_T > Q_T^{sep}$ and $Q_T < Q_T^{sep}$ should not depend on Q_T^{sep}. As shown in Fig. 3(b), the NLO total cross section indeed does not depend on the choice of

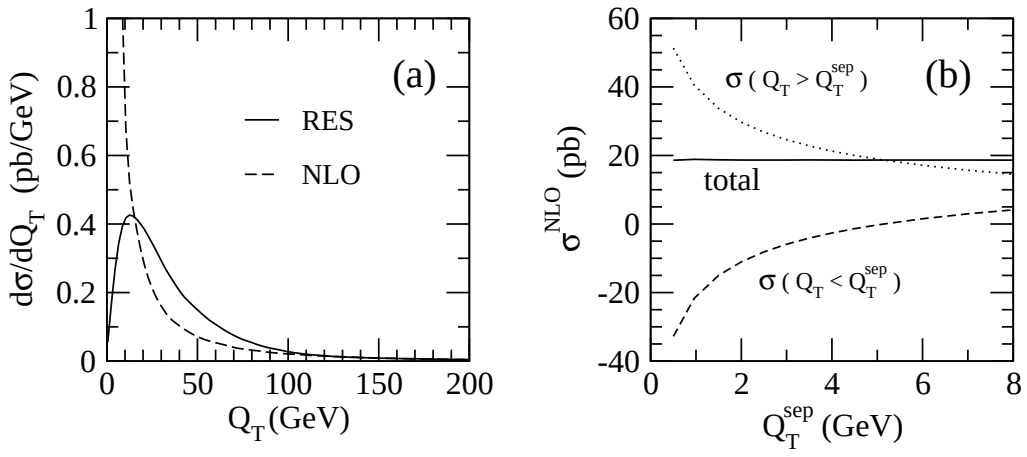

Figure 3: (a) Distribution of transverse momentum of Higgs boson, and (b) NLO total production cross section of Higgs boson via gluon gluon fusion as $M_H = 170\,\text{GeV}$ at the LHC.

Q_T^{sep} as long as it is not too large. We refer the readers to the Sec. 3 and the Appendix of Ref. [43] for more details. In this study, we choose $Q_T^{sep} = 0.96\,\text{GeV}$ in our numerical calculations.

As mentioned in the Introduction, MC@NLO, which matches NLO calculations and parton showering Monte Carlo event generators, not only predicts a reliable Q_T of the Higgs boson but also includes spin correlations among the Higgs decay products. Therefore it is interesting to compare the Q_T predictions between MC@NLO and RES calculations. In order to compare the differences in shape more precisely, we show the Q_T distributions predicted by MC@NLO and ResBos in Fig. 4 for $M_H = 140(\,170,\,200,\,600)\,\text{GeV}$. All distributions are normalized by the total cross sections for the corresponding Higgs boson masses. The bottom part of each Q_T distribution plot presents the ratio between MC@NLO and ResBos. We note that for a light Higgs boson the distributions are consistent in the peak region [34, 36], where the difference is about 10 %, but they are quite different in the large Q_T region, say $Q_T \gtrsim 100\,\text{GeV}$. For a heavy Higgs boson, e.g. $M_H = 600\,\text{GeV}$, these two distributions are very different in the small Q_T region, and MC@NLO tends to populate more events in the small Q_T region, as compared to ResBos. Since the Higgs boson is a scalar, the distributions of Higgs boson decay products just depend upon the Higgs boson's kinematics. Therefore, the difference in the Q_T distribution predictions between MC@NLO and ResBos may prove to be crucial for the precision measurements of the Higgs boson's properties. A further detailed study of the impact of the Q_T difference on the Higgs boson search is in

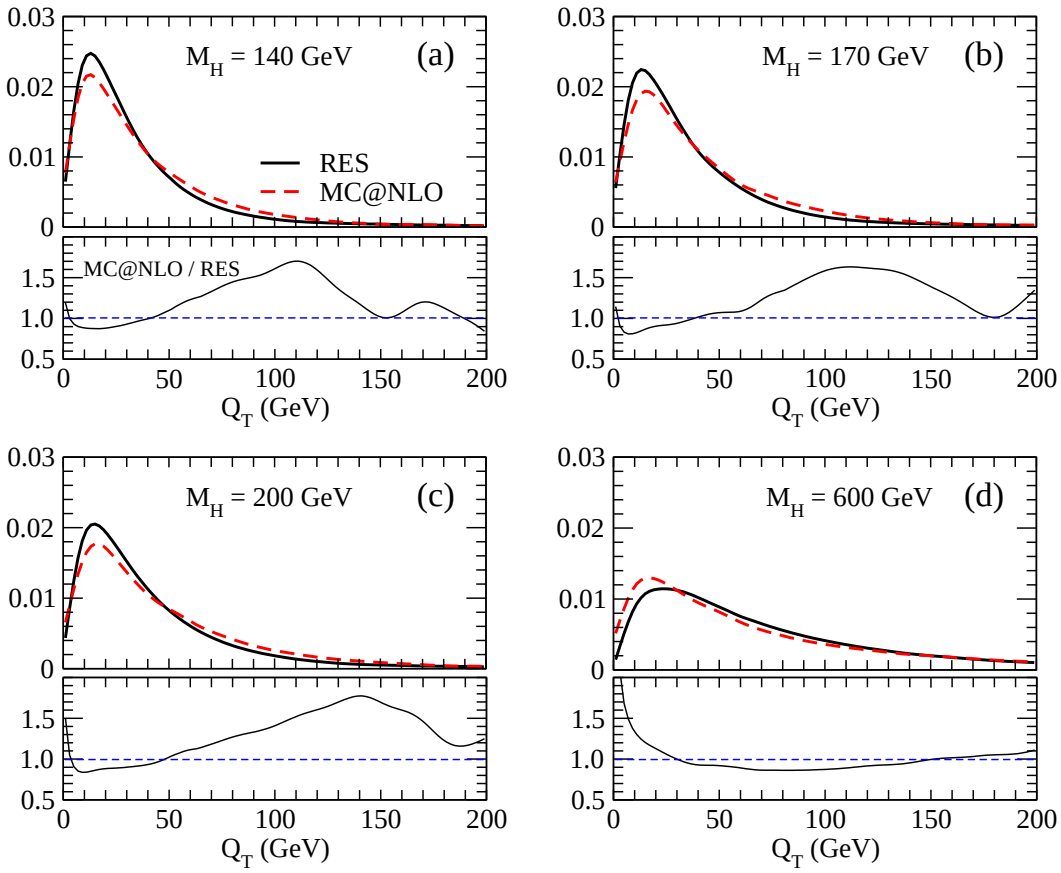

Figure 4: Comparison of the Q_T distributions between ResBos and MC@NLO.

order and will be presented elsewhere.

IV. PHENOMENOLOGICAL STUDY OF THE $H \to WW$ MODE

In the search for SM-like Higgs boson via $H \to WW^{(*)}$ mode, two scenarios of W boson decay were considered in the literature [60, 61, 62]: one is that both W bosons decay leptonically, another is that one W boson decays leptonically and another W boson decays hadronically. Throughout this paper, we only concentrate on the di-lepton decay mode, i.e. $H \to WW^{(*)} \to \ell^+\ell'^-\nu_\ell\bar{\nu}_{\ell'}$, at the Tevatron and the LHC. The collider signature, therefore, is two isolated opposite-sign charged leptons plus large missing transverse energy ($\not\!\!E_T$) which originates from the two neutrinos. In this section, we first examine the RES effects on various kinematics distributions, and then show the RES effects on the Higgs mass measurement. Finally, we study the RES effects on the acceptances of the kinematics cuts suggested in the literature for Higgs search.

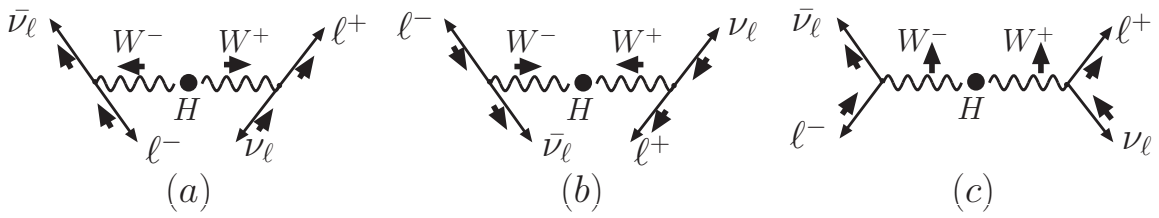

Figure 5: Kinematic configurations of Higgs decay ($H \to WW \to \ell^+\ell^-\nu\bar{\nu}$) in the rest frame of H: (a) $H \to W^+_+W^-_+$, (b) $H \to W^+_-W^-_-$ and (c) $H \to W^+_0W^+_0$. Here, $+(-,\, 0)$ denotes the right-handed (left-handed, longitudinal) polarization state of the W boson. The long arrows denote the moving directions of the final-state leptons. The short bold arrows denote the particles' spin directions.

A. Basic kinematics distributions

For a heavy Higgs boson, the two vector bosons, which are generated from the spin-0 Higgs boson decay, are predominantly longitudinally polarized, while the longitudinal and transverse polarization states are democratically populated when the Higgs boson mass is near the threshold for decaying into the vector boson pair [63, 64]. When $140\,\text{GeV} \leq M_H \leq 170\,\text{GeV}$, the transverse polarization modes contribute largely. The two charged leptons in the final state have different kinematics because of the conservation of angular momentum, cf. Fig. 5, therefore, one charged lepton is largely boosted and its momentum becomes harder while another becomes softer. Making use of these differences, one can impose asymmetric transverse momentum (p_T) cuts on the two charged leptons to suppress the background. On the event-by-event basis, we arrange the two charged leptons in the order of transverse momentum: $p_T^{L_{max}}$ denotes the larger p_T between the two charged leptons while p_T^L is the smaller one. Fig. 6 shows the distributions of $p_T^{L_{max}}$, p_T^L and missing energy ($\not{E}_T$) for $M_H = 140\,\text{GeV}$ at the Tevatron (first row) and for $M_H = 170\,\text{GeV}$ at the LHC (second row). Furthermore, in Fig. 7 we show the distributions of $\cos\theta_{LL}$, ϕ_{LL} and ΔY_{LL} without imposing any kinematics cut, where $\cos\theta_{LL}$ is the cosine of the opening angle between the two charged leptons, ϕ_{LL} is the azimuthal angle difference between the two charged leptons on the transverse plane, and ΔY_{LL} is the rapidity difference of two charged leptons in the lab frame. Since we are mainly interested in the shapes of the kinematics distributions, the curves shown in the figures are all normalized by the corresponding total cross sections. The solid curves present the distributions including the RES effects, the dashed and dotted curves present

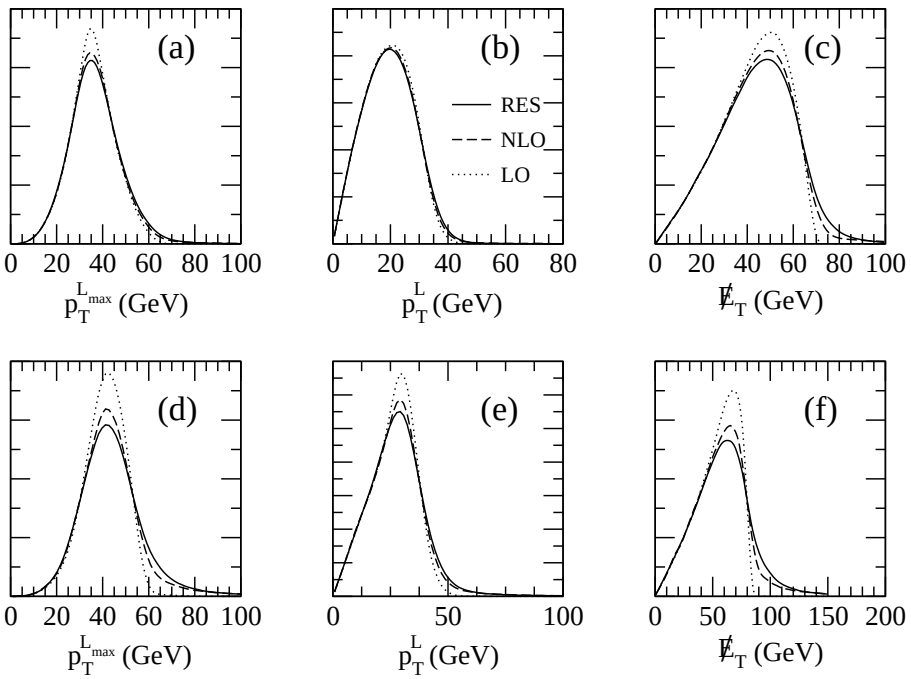

Figure 6: Normalized distributions of the leading transverse momentum $p_T^{L_{max}}$, softer transverse momentum p_T^L of the leptons, and the missing energy $\not{E}_T$ in $gg \to H \to WW \to \ell^+\ell'^-\nu_\ell\bar{\nu}_{\ell'}$. The panels (a) to (c) are for $M_H = 140\,\text{GeV}$ at the Tevatron, and (d) to (f) are for $M_H = 170\,\text{GeV}$ at the LHC.

the distributions calculated at the NLO and LO, respectively.

We note that the p_T distributions of the charged leptons and the missing energy distributions are modified largely by the RES effects. This can be understood as follows. The two charged leptons prefer to move in the same direction due to the spin correlation among the decay products of the Higgs boson, cf. the distributions of $\cos\theta_{LL}$ in Figs. 7(a) and (d). Hence, one can approximately treat the Higgs boson decay as "two-body" decay, i.e. decaying into two clusters as $H \to (\ell^+\ell'^-)\,(\nu_\ell\bar{\nu}_{\ell'})$. This is in analogy to the W boson production and decay in the Drell-Yan process, $u\bar{d} \to W^+ \to \ell^+\nu$, which has been shown in Ref. [51] that the transverse momentum of lepton (p_T^ℓ) is very sensitive to the transverse momentum of the W boson. The same sensitivity also applies to $\not{E}_T$. As shown in Figs. 6(c) and (f), the clear Jacobian peak of the $\not{E}_T$ distribution around $M_H/2$ in the LO calculation is smeared in the NLO and RES calculations. Furthermore, the $\not{E}_T$ distribution in the NLO and RES calculations has a long tail due to the non-zero transverse momentum of the Higgs boson. Since the RES calculation includes the effects from multiple soft-gluon radiation, the $\not{E}_T$

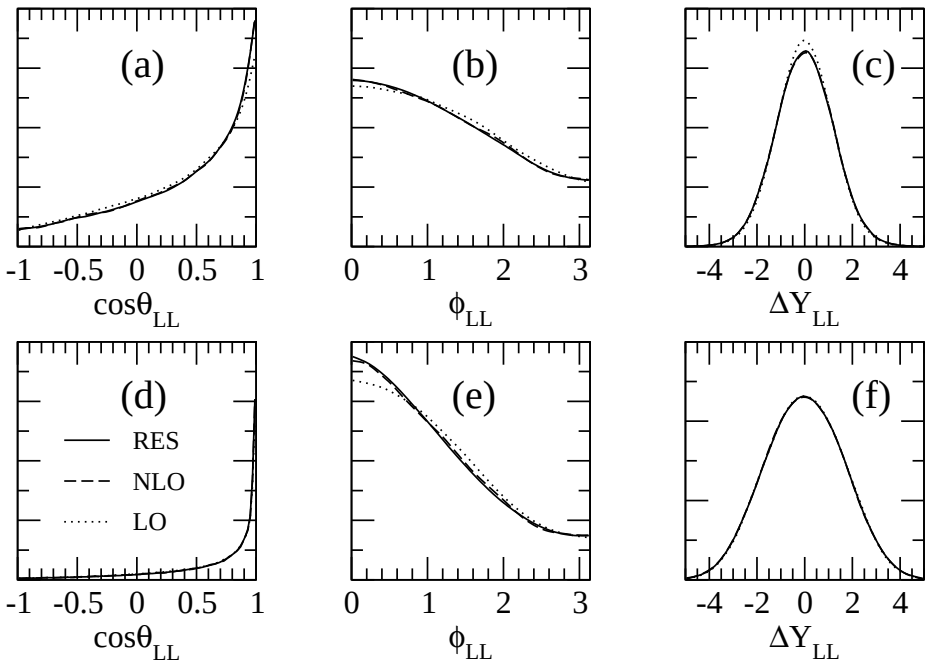

Figure 7: Normalized distributions of $\cos\theta_{LL}$, ϕ_{LL} and ΔY_{LL} in $gg \to H \to WW \to \ell^+\ell'^-\nu_\ell\bar{\nu}_{\ell'}$: The panels (a) to (c) are for $M_H = 140\,\mathrm{GeV}$ at the Tevatron and (d) to (f) are for $M_H = 170\,\mathrm{GeV}$ at the LHC.

distribution near the Jacobian peak is further smeared in the RES calculation as compared to the NLO calculation. When $M_H = 140\,\mathrm{GeV}$, only one W boson is on-shell and the two charged leptons do not move as close as they do in the case of $M_H = 170\,\mathrm{GeV}$ (in which case, both W bosons are on-shell). However the parallel configuration is still preferred.

The dominant backgrounds of the $H \to WW^{(*)}$ mode are from the W boson pair production and top quark pair production. The latter, as the reducible background, can be suppressed with suitable cuts such as jet-veto, but the former, as the irreducible background, still remains even after imposing the basic kinematic cuts. In order to reduce this intrinsic background, one needs to take advantage of the characteristic spin correlations of the charged leptons in the $H \to WW^{(*)} \to \ell^+\ell'^-\nu_\ell\bar{\nu}_{\ell'}$ decay. For example, the distribution of the difference in azimuthal angles of the charged leptons peaks at smaller value (cf. Figs. 7(b) and (e)) for the signal than that for the WW continuum production background [60, 62]. We note that the RES effects do not affect the $\cos\theta_{LL}$ and ϕ_{LL} distributions very much, as shown in Figs. 7(a), (b), (d) and (e).

To closely examine the difference in their predictions, we also present the ratio of the RES

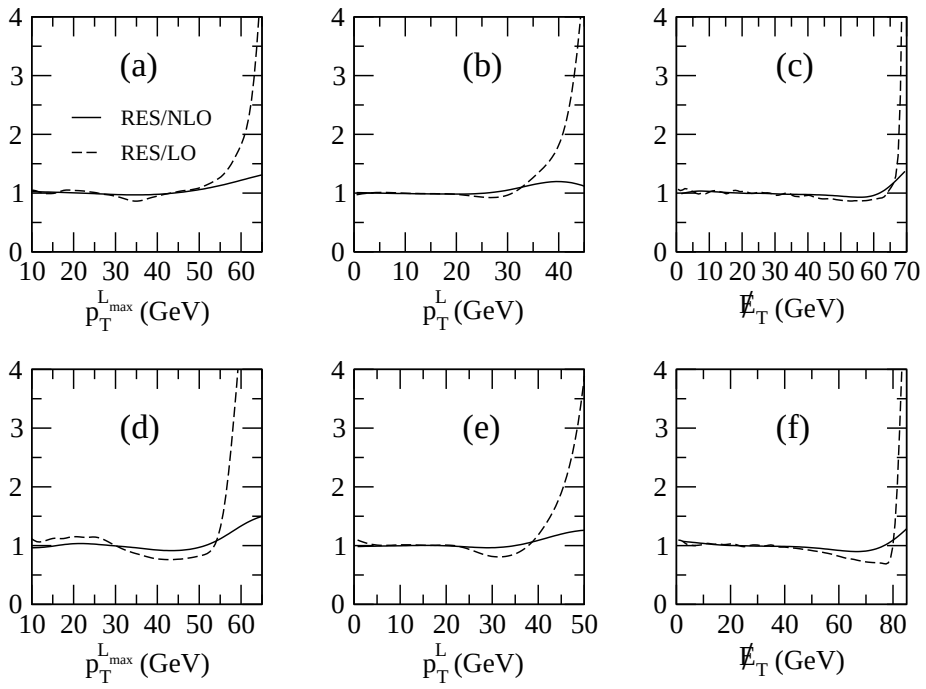

Figure 8: Ratio of the Resummation contribution to NLO and LO contributions in $gg \to H \to WW^{(*)} \to \ell^+\ell'^-\nu_\ell\bar{\nu}_{\ell'}$. The panels (a) to (c) are for $M_H = 140\,\mathrm{GeV}$ at the Tevatron while (d) to (f) are for $M_H = 170\,\mathrm{GeV}$ at the LHC.

contribution to the NLO and LO contributions in Fig. 8. We note that the ratio is about one below the peak regions of $p_T^{L_{max}}$, p_T^L and $\not\!\!E_T$, and becomes larger than one above the peak region, where both the LO and NLO contributions drop faster than the RES contribution does, which is consistent with the results shown in Fig. 6. This uneven behavior indicates that one cannot simply use the leading order kinematics with the constant K-factor included to mimic the higher order quantum corrections. We should stress that even though the NLO and RES calculations include the same contributions of the hard gluon radiation from initial states, the effects of the multiple soft-gluon radiation could cause more than 25% difference between RES and NLO predictions in the large p_T and $\not\!\!E_T$ region.

B. Higgs mass measurement

In order to identify the signal events clearly, it is crucial to reconstruct the invariant mass of the Higgs boson. Unfortunately, one cannot directly reconstruct the M_H distribution in the $H \to WW$ mode due to the two neutrinos in the final state. Instead, both the transverse

mass M_T and the cluster transverse mass M_C [65], defined as

$$\begin{aligned} M_T &= \sqrt{2p_T^{LL} \not{E}_T(1-\cos\Delta\phi(p_T^{LL},\not{E}_T))}, \\ M_C &= \sqrt{p_T^{LL^2}+m_{LL}^2}+\not{E}_T, \end{aligned} \tag{3}$$

yield a broad peak near M_H. In Eq. (3), p_T^{LL} (m_{LL}) denotes the transverse momentum (invariant mass) of the two charged lepton system, and $\Delta\phi(p_T^{LL}, \not{E}_T)$ is the difference in azimuthal angles between p_T^{LL} and $\not{E}_T$ on the transverse plane. We note that the upper endpoint of M_T distribution can clearly reflect the mass of Higgs boson, cf. Figs. 9(a) and (c). M_T is insensitive to Q_T because it depends on Q_T in the second order, cf. Eq. (3). Therefore, the position of the endpoint is only subject to M_H and Γ_H. The latter effects can be safely ignored because Γ_H is very small (less than about 1.5 GeV), for the Higgs boson mass less than 200 GeV. The cluster transverse mass M_C also exhibits a clear Jacobian peak with a clear edge at M_H, cf. Figs. 9(b) and (d). But both the line shape and the Jacobian peak of M_C distribution are modified by the RES effects because M_C is directly related to $\not{E}_T$ which depends on Q_T in the first order. We suggest that one should use M_T to extract the mass of Higgs in $H \to WW^{(*)} \to \ell^+\ell'^-\nu_\ell\bar{\nu}_{\ell'}$ mode because the upper endpoint of the M_T distribution is insensitive to high order corrections.

C. Acceptance study

In order to separate the signal from its copious backgrounds, one needs to impose optimal cuts to suppress backgrounds and enhance the signal to background ratio (S/B) simultaneously. The selection of the optimal cuts highly depends on how well we understand the kinematics of the signal and background processes. As shown above, the RES effects modify the distributions of transverse momentum of the charged leptons and the missing energy largely, therefore, it is important to study the RES effects on the acceptances of the kinematics cuts. Here, we impose a set of kinematics cuts used by experimental colleagues in Refs. [37, 39]. The corresponding acceptances are summarized in Table II.

- For the search for a 140 GeV Higgs boson at the Tevatron, we impose the following *basic cuts*:

$$\begin{aligned} p_T^{L_{max}} > 15\,\text{GeV}\ ,\ p_T^L > 10\,GeV, \\ |Y_L| < 2.0\ ,\ \not{E}_T > 20\,\text{GeV}, \end{aligned} \tag{4}$$

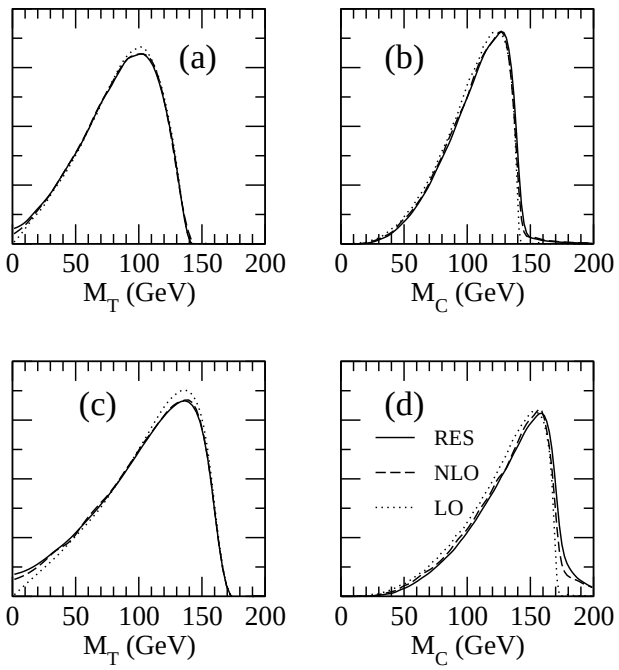

Figure 9: Normalized distributions of the transverse mass M_T and the cluster mass M_C in $gg \to H \to WW^{(*)} \to \ell^+\ell'^-\nu_\ell\bar{\nu}_{\ell'}$: (a) and (b) are for $M_H = 140\,\mathrm{GeV}$ at the Fermilab Tevatron while (c) and (d) are for $M_H = 170\,\mathrm{GeV}$ at the LHC.

and the *optimal cuts* as follows:

$$\begin{aligned} m_{LL} < \frac{M_H}{2} \ , \ \frac{M_H}{2} < M_T < M_H - 10\,\mathrm{GeV} \\ \phi_{LL} < 2.0\,\mathrm{rad} \ , \ \frac{M_H}{2} + 20\,GeV < H_T < M_H \end{aligned} \tag{5}$$

where Y_L denotes the rapidity of charged lepton, and H_T denotes the scalar sum of the transverse momenta of final state particles, i.e. $H_T \equiv |p_T^e| + |p_T^\mu| + |\not{E}_T|$. The overall efficiency of the cuts is about 68% , 69% and 70% after imposing the basic cuts (Eq. (4)) for RES, NLO and LO calculations, respectively, and about 44% for both RES and NLO calculations and 46% for LO calculation after imposing the optimal cuts (Eq. (5)).

- For the search of a 170 GeV Higgs boson at the LHC, we require the following *basic cuts*:

$$\begin{aligned} p_T^{L_{max}} > 20\,\mathrm{GeV} \ , \ p_T^L > 10\,\mathrm{GeV}, \\ |Y_L| < 2.5 \ , \ \not{E}_T > 40\,\mathrm{GeV}, \end{aligned} \tag{6}$$

Table II: Acceptance of $gg \to H \to WW^{(*)} \to \ell^+\ell'^-\nu_\ell\bar{\nu}_{\ell'}$ events after imposing the basic cuts and the optimal cuts for $M_H = 140\,\text{GeV}$ at the Tevatron and $M_H = 170\,\text{GeV}$ at the LHC.

	$M_H = 140\,\text{GeV}$		$M_H = 170\,\text{GeV}$	
	basic (Eq. (4))	optimal (Eq. (5))	basic (Eq. (6))	optimal (Eq. (7))
RES	0.68	0.44	0.61	0.19
NLO	0.69	0.44	0.61	0.19
LO	0.70	0.46	0.63	0.20

and the *optimal cuts*:

$$m_{LL} < 80.0\,\text{GeV}\ ,\ M_H - 30.0\,\text{GeV} < M_T < M_H\,,$$
$$\phi_{LL} < 1.0\,\text{rad}\ ,\ \theta_{LL} < 0.9\,\text{rad}\ ,\quad |\Delta Y_{LL}| < 1.5\ , \tag{7}$$

The cut efficiency is about 61% for both RES and NLO calculations, but about 63% for LO contribution after imposing the basic cut (Eq. (6)). After imposing the optimal cuts (Eq. (7)), the acceptances of RES and NLO are about 19%, while LO is 20%.

V. PHENOMENOLOGICAL STUDY OF THE $H \to ZZ$ MODE

In the search for the SM Higgs boson, the $H \to ZZ^{(*)} \to \ell^+\ell^-\ell'^+\ell'^-$ is an important discovery channel for a wide range of Higgs boson mass. The appearance of four charged leptons with large transverse momenta is an attractive experimental signature. This so-called "gold-plated" mode provides not only a clean signature to verify the existence of the Higgs boson but also an excellent process to explore its spin and CP properties [66]. In this section, we study three mass values of M_H (140, 200 and 600 GeV) at the LHC. For $M_H = 140\,\text{GeV}$ and $200\,\text{GeV}$, we require the two Z bosons both decay into charged leptons; for $M_H = 600\,\text{GeV}$, we require one Z boson decays into a charged lepton pair and another Z boson decays into a neutrino pair, i.e. $\ell^+\ell^-\nu\bar{\nu}$. In this section we first study the RES effects on various kinematics distributions and then examine the RES effects on the acceptances of the kinematics cuts.

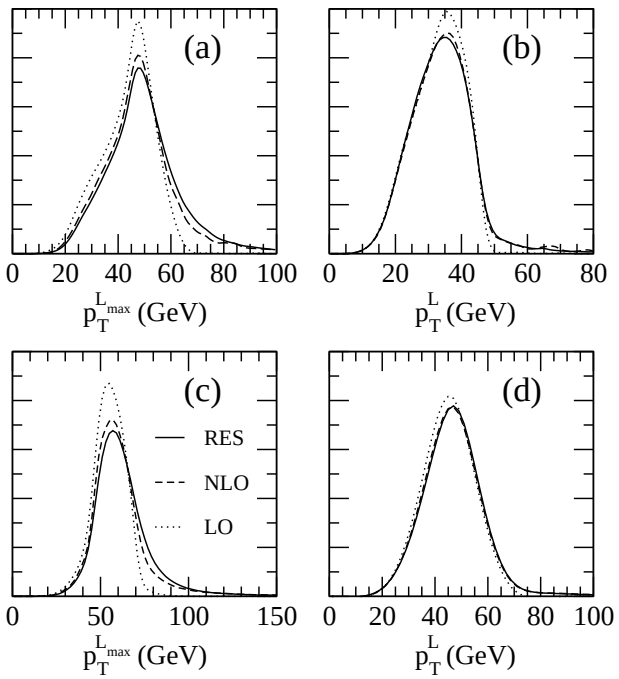

Figure 10: Normalized distributions of $p_T^{L_{max}}$ and p_T^L in $gg \to H \to ZZ \to \ell^+\ell^-\ell'^+\ell'^-$: (a) and (b) are for $M_H = 140\,\text{GeV}$; (c) and (d) are for $M_H = 200\,\text{GeV}$ at the LHC.

A. $gg \to H \to ZZ^{(*)} \to \ell^+\ell^-\ell'^+\ell'^-$

Similar to the $H \to WW^{(*)}$ mode, we also arrange the four charged leptons of the $H \to ZZ^{(*)}$ mode in the order of transverse momentum. We denote $p_T^{L_{max}}$ as the largest p_T of the four charged leptons while p_T^L the second leading p_T. In Fig. 10, we show the distributions of $p_T^{L_{max}}$ and p_T^L for $M_H = 140$ and $200\,\text{GeV}$, respectively. Due to the similar kinematics discussed in the $H \to WW^{(*)}$ mode, the shapes of the distributions of $p_T^{L_{max}}$ and p_T^L are changed significantly by the RES effects. The typical feature is that the RES effects shift the p_T of the charged lepton to the larger p_T region and, therefore, increase the acceptances of the kinematics cuts. The numerical results will be shown later.

Although one can measure the Higgs boson mass by reconstructing the invariant mass of the four charged leptons, one still needs to reconstruct the Z bosons in order to suppress the backgrounds. The reconstruction of the Z boson depends on the lepton flavors in the final state. In this study, we consider two scenarios: different flavor charged lepton pairs, i.e. $H \to 2e2\mu$, and four same flavor charged leptons, i.e. $H \to 4e(\text{ or } 4\mu)$. Hence, we have two methods for reconstructing the Z bosons:

1. Different flavor charged lepton pairs ($2e2\mu$):
   In this case, it is easy to reconstruct the Z bosons because both electron and muon lepton flavors can be tagged. Using the flavor information, the Z bosons can be reconstructed by summing over the same flavor opposite-sign leptons in the final state.

2. Four same flavor charged leptons ($4e/4\mu$):
   If the flavors of four leptons are all the same, one needs to pursue some algorithms to reconstruct the Z boson mass. In our analysis, we first pair up the leptons with opposite charge. We require the pair whose invariant mass is closest to M_Z to be the one generated from the on-shell Z boson, and the other pair is the one generated from another Z boson, which could be on-sell or off-shell. We name it as the minimal deviation algorithm (MDA) in this paper.

In Fig. 11, we show the p_T distributions of the reconstructed Z boson for 140 and 200 GeV, respectively. When the final state lepton flavors are different, one can reconstructed the Z boson perfectly by matching the lepton flavor. For the same flavor leptons, the reconstructed Z boson distributions in the MDA are shown as the solid, dashed and dot-dashed curves for RES, NLO and LO, respectively. Some points are worthy to point out as follow:

- We note that the MDA can perfectly reconstruct the distributions of true Z bosons, irregardless whether these two Z bosons are both on-shell or only one of them is on-shell.

- When $M_H = 200\,\text{GeV}$, both Z bosons are produced on-shell and boosted. The peak position of the transverse of momentum p_T^Z is around $\sqrt{(M_H/2)^2 - m_Z^2} \sim 41\,\text{GeV}$. For all the cases, the RES effects change the shape of p_T^Z largely and shift the p_T^Z to the larger value region.

It has been shown in Ref. [67] that angular correlation between the two Z bosons from the Higgs decay can be used to suppress the intrinsic background from ZZ pair production efficiently. One of the useful angular variables is the polar angle (θ_Z^*) of the (back-to-back) Z boson momenta in the rest frame of the Higgs boson [67]. As shown in Fig. 12, in the rest frame of Higgs boson, the back-to-back Z bosons like to lie in the direction perpendicular to the $z-$axis, which is the moving direction of the Higgs boson in the lab frame. After being

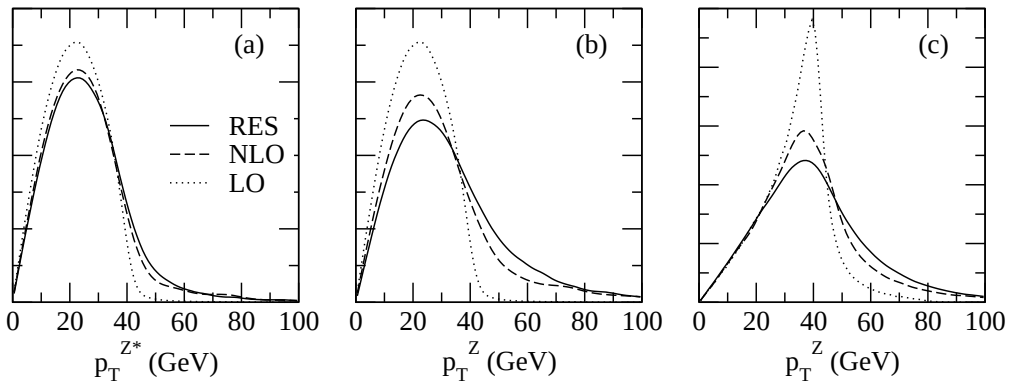

Figure 11: Normalized transverse momentum of Z boson in $gg \to H \to ZZ^{(*)} \to \ell^+\ell^-\ell'^+\ell'^-$ at the LHC: (a) is the p_T distributions of off-shell Z boson for $M_H = 140\,\text{GeV}$, (b) is the p_T distributions of on-shell Z boson for $M_H = 140\,\text{GeV}$ and (c) is the p_T distributions of on-shell Z boson for $M_H = 200\,\text{GeV}$.

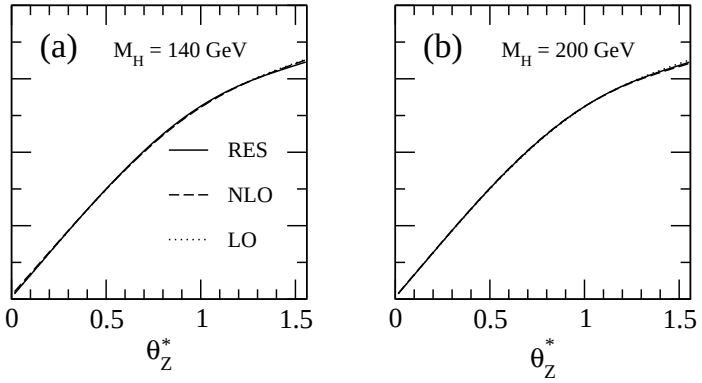

Figure 12: Normalized polar angle of the (back-to-back) Z boson momenta distributions in the rest frame of the Higgs boson in $gg \to H \to ZZ^{(*)} \to \ell^+\ell^-\ell'^+\ell'^-$ at the LHC: (a) is for $M_H = 140\,\text{GeV}$, (b) is for $M_H = 200\,\text{GeV}$.

boosted to the lab frame, two Z bosons will move close to each other, c.f. Fig. 13(b), where θ_{ZZ} is the opening angle between the two Z bosons in the lab frame. Another interesting angular variable is the angle between the two on-shell Z boson decay planes (ϕ_{DP}) in the rest frame of the Higgs boson, which is shown in Fig. 13(a). The two Z bosons are reconstructed as explained above. Since the angle θ_Z^* and ϕ_{DP} are defined in the rest frame of the Higgs boson, the non-zero transverse momentum of the Higgs boson does not affect these two variables. Therefore, as clearly shown in the figures, all the distributions of the angular variables mentioned above are the same for the RES, NLO and LO calculations.

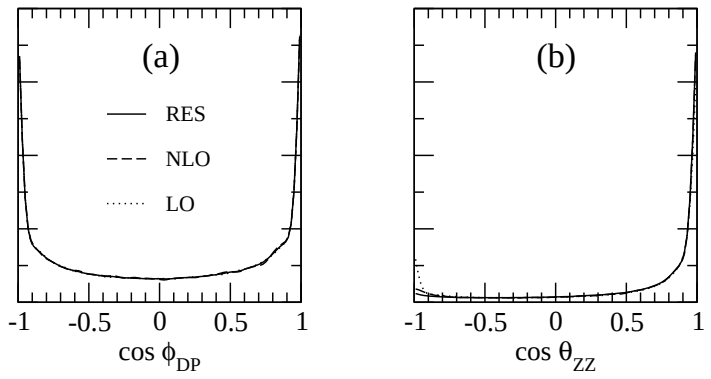

Figure 13: Normalized distributions of $\cos\phi_{DP}$ and $\cos\theta_{ZZ}$ in the rest frame of the Higgs boson with mass 200 GeV in $gg \to H \to ZZ \to \ell^+\ell^-\ell'^+\ell'^-$ at the LHC.

B. $gg \to H \to ZZ \to \ell^+\ell^-\nu\bar{\nu}$

Although the "gold-plated" mode, $H \to ZZ \to \ell^+\ell^-\ell'^+\ell'^-$, is considered to be the most effective channel for the SM Higgs boson discovery at the LHC, it suffers from the small decay branching of $Z \to \ell^+\ell^-$. Moreover, the larger the Higgs mass becomes, the smaller the production rate is. When the Higgs boson mass is larger than 600 GeV, the $H \to ZZ \to \ell^+\ell^-\nu\bar{\nu}$ channel may become important because the decay branching ratio (Br) of $H \to ZZ \to \ell^+\ell^-\nu\bar{\nu}$ is six times of the Br of $H \to ZZ \to \ell^+\ell^-\ell'^+\ell'^-$. The drawback is that one cannot reconstruct the Higgs mass from the final state particles due to the presence of two neutrinos. In this discovery channel, the missing transverse energy ($\not{E}_T$) is crucial to suppress the background [37]. The $\not{E}_T$ distribution is shown in Fig. 14(a) which exhibits a Jacobian peak around $M_H/2$, and the soft-gluon resummation effects smear the Jacobian peak and shift more events to the larger $\not{E}_T$ region. Similar to the $H \to WW$ mode, the kinematics of this channel is similar to the W boson production and decay in the Drell-Yan process, therefore the shape of $\not{E}_T$ distribution change significantly by the RES contributions. The Higgs boson mass can be measured from the peaks of the distributions of the transverse mass M_T and the cluster mass M_C, cf. Eq. (3), as shown in Fig. 14(b) and (c). Although the upper endpoint of M_T is insensitive to high order corrections as we mentioned in the study of $H \to WW^{(*)}$ mode, the Jacobian peak is smeared out by the width (Γ_H) effects of the Higgs boson. For $M_H = 600$ GeV, the total decay width of the Higgs boson is about

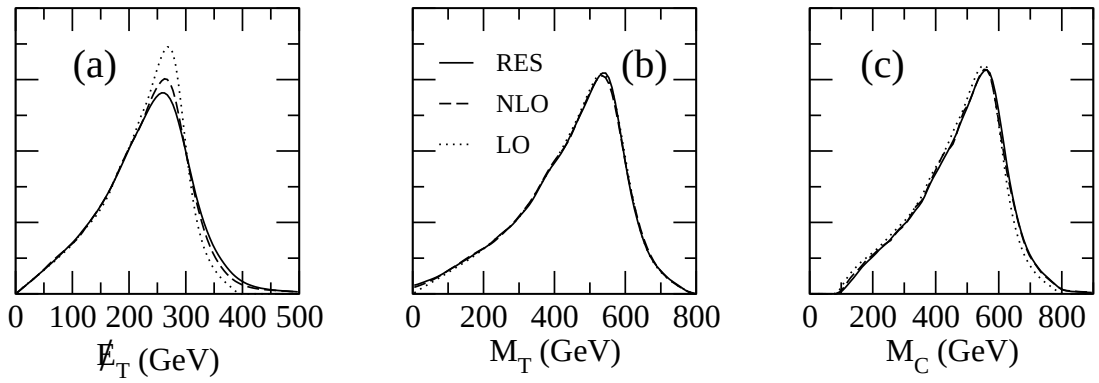

Figure 14: Normalized distributions of $\not{E}_T$, M_T and M_C in $gg \to H \to ZZ \to \ell^+\ell^-\nu\nu$ channel with $M_H = 600\,\text{GeV}$ at the LHC.

Table III: Acceptance of the process $gg \to H \to ZZ \to \ell^+\ell^-\ell'^+\ell'^-$ for $M_H = 140\,(200)\,\text{GeV}$ and the process $gg \to H \to ZZ \to \ell^+\ell^-\nu\bar{\nu}$ for $M_H = 600\,\text{GeV}$ after imposing cuts.

	$M_H = 140\,\text{GeV}$		$M_H = 200\,\text{GeV}$		$M_H = 600\,\text{GeV}$
	basic (Eq. 8)	optimal (Eq. 9)	basic (Eq. 8)	optimal (Eq. 9)	basic (Eq. 10)
RES	0.53	0.15	0.67	0.14	0.55
NLO	0.54	0.12	0.67	0.11	0.56
LO	0.53	0	0.67	0	0.58

120 GeV, which is quite sizable and generates a noticeable smearing effect on the Jacobian peak.

C. Acceptance study

The discovery potential of the $H \to ZZ \to \ell^+\ell^-\ell'^+\ell'^-$ and $H \to ZZ \to \ell^+\ell^-\nu\bar{\nu}$ modes has been studied in Ref. [37] after imposing the following cuts:

- For $M_H = 140\,\text{GeV}$ and $200\,\text{GeV}$, the intermediate mass range, we impose the *basic cuts*:

$$p_T^E > 7.0\,\text{GeV},\ |Y_L| < 2.5,\ p_T^L > 20\,\text{GeV}, \tag{8}$$

  and the *optimal cuts*:

$$p_T^{Z_{Max}} > \frac{M_H}{3}, \tag{9}$$

where p_T^E and Y_L are the transverse momentum and rapidity of each charged lepton, respectively, and $p_T^{Z_{Max}}$ is the p_T of the harder Z boson.

- For $M_H = 600\,\mathrm{GeV}$, we require:

$$p_T^L > 40\,\mathrm{GeV}, \quad |Y_L| < 2.5\,,$$
$$p_T^{LL} > 200\,\mathrm{GeV}, \quad \not{E}_T > 150\,\mathrm{GeV}, \tag{10}$$

where p_T^{LL} is the transverse momentum of the two charged lepton system. The numerical results of the acceptances of the various cuts are summarized in Table III. For the $H \to ZZ^{(*)} \to \ell^+\ell^-\ell'^+\ell'^-$ mode, the RES and NLO contributions have almost the same acceptances after imposing the basic cuts. However, after imposing the optimal cuts the acceptance of the RES contribution is larger than the one of the NLO contribution by 25%, and the LO contribution is largely suppressed. For the $H \to ZZ \to \ell^+\ell^-\nu\bar{\nu}$ mode, the acceptances of the RES and NLO calculations are similar to each other.

VI. CONCLUSION

The search for the SM Higgs boson is one of the major goals of the high energy physics experiments at the LHC, and the vector boson decay modes, $H \to WW^{(*)}$ or $H \to ZZ^{(*)}$, provide powerful and reliable discovery channels. The LHC has a great potential to discover the Higgs boson even with low luminosity ($\sim 30\,\mathrm{fb}^{-1}$) during the early years of running [37, 38, 68]. In order to extract the signal from huge background events, we should have better theoretical predictions of the signal events as well as background events. In this paper, we examine the soft gluon resummation effects on the search of SM Higgs boson via the dominant production process $gg \to H$ at the LHC and discuss the impacts of the resummation effects on various kinematics variables which are relevant to the Higgs search. A comparison between the resummation effects and the NLO calculation is also presented.

For $H \to WW^{(*)} \to \ell^+\ell^-\nu\bar{\nu}$ mode, we study $M_H = 140\,\mathrm{GeV}$ at the Tevatron and $M_H = 170\,\mathrm{GeV}$ at the LHC. Due to the spin correlations between the final state particles, this process is similar to the W boson production and decay in the Drell-Yan process. The shapes of the kinematics distributions are modified significantly by RES effects. For example, the effects could cause $\sim 50\%$ difference compared to NLO calculation in the

transverse momentum distribution of the leading lepton ($p_T^{L_{Max}}$), when $M_H = 170\,\text{GeV}$. The Higgs boson mass cannot be reconstructed directly from the final state particles because of two neutrinos. Therefore, the upper endpoint in the transverse mass distribution can be used to determine the mass of the Higgs boson, and we found that it is insensitive to the RES effects. After imposing various kinematics cuts, the LO, NLO and RES calculations yield similar acceptance of the signal events.

For the $H \to ZZ^{(*)} \to \ell^+\ell^-\ell'^+\ell'^-$ mode, the so-called "gold-plated" mode, we study $M_H = 140\,\text{GeV}$ and $M_H = 200\,\text{GeV}$ at the LHC in this paper. We pursue an algorithm, called minimal deviation algorithm in this paper, to reconstruct the two Z bosons when the four charged leptons in the final state have the same flavors. The RES effects change the shapes of kinematics significantly, e.g. $p_T^{L_{max}}$ and p_T^Z distributions. However, the variables ϕ_{DP} and θ_Z^*, defined in the Higgs rest frame, are insensitive to RES effects. After imposing the optimal kinematics cuts, the RES effects could increase the acceptance by 25% compared to that of NLO calculation while the LO contribution is largely suppressed. When the Higgs boson is heavy (600 GeV), we consider the $H \to ZZ \to \ell^+\ell^-\nu\bar{\nu}$ mode because of its larger decay branching ratio, as compared to the $H \to ZZ \to \ell^+\ell^-\ell'^+\ell'^-$ mode. The shape of $\not{E}_T$ distribution, which is crucial to suppress the backgrounds, is largely modified because it is sensitive to the transverse momentum of the Higgs boson.

In summary, we have presented a study of initial state soft-gluon resummation effects on the search for the SM Higgs boson via gluon-gluon fusion at the LHC. The effects not only significantly modify some of the kinematic distributions of the final state particles, as compared to the NLO and LO predictions, but also enhance the acceptance of the signal events after imposing the kinematic cuts to suppress the large background events. Therefore, we conclude that the initial state soft-gluon resummation effects should be taken into account as searching for the Higgs boson at the LHC. In addition, we note that the spin correlations among the final state leptons could be modified by the electroweak corrections to the Higgs boson decay. Therefore, we have implemented the NLO QED correction in the ResBos code, and the phenomenological study will be presented in the forthcoming paper.

Acknowledgments

We thank Professor C.-P. Yuan for a critical reading and useful suggestions. We also thank Dr. Kazuhiro Tobe for useful discussions. Q.-H. Cao is supported in part by the U.S. Department of Energy under grant No. DE-FG03-94ER40837. C.-R. Chen is supported in part by the U.S. National Science Foundation under award PHY-0555545.

---

[1] R. Barate et al. (LEP Working Group for Higgs boson searches), Phys. Lett. **B565**, 61 (2003), hep-ex/0306033.

[2] http://lepewwg.web.cern.ch.

[3] See, e.g., T. Hambye, and K. Riesselmann, Phys. Rev. **D55**, 7255 (1997), hep-ph/9610272.

[4] D. Froidevaux, F. Gianotti, and E. Richter Was (1995), ATLAS Note PHYS-NO-064.

[5] F. Gianotti and I. Vichou (1996), ATLAS Note PHYS-NO-078.

[6] S. Dawson, Nucl. Phys. **B359**, 283 (1991).

[7] A. Djouadi, M. Spira, and P. M. Zerwas, Phys. Lett. **B264**, 440 (1991).

[8] M. Spira, A. Djouadi, D. Graudenz, and P. M. Zerwas, Nucl. Phys. **B453**, 17 (1995), hep-ph/9504378.

[9] M. Kramer, E. Laenen, and M. Spira, Nucl. Phys. **B511**, 523 (1998), hep-ph/9611272.

[10] R. V. Harlander, Phys. Lett. **B492**, 74 (2000), hep-ph/0007289.

[11] S. Catani, D. de Florian, and M. Grazzini, JHEP **05**, 025 (2001), hep-ph/0102227.

[12] R. V. Harlander and W. B. Kilgore, Phys. Rev. **D64**, 013015 (2001), hep-ph/0102241.

[13] R. V. Harlander and W. B. Kilgore, Phys. Rev. Lett. **88**, 201801 (2002), hep-ph/0201206.

[14] C. Anastasiou and K. Melnikov, Nucl. Phys. **B646**, 220 (2002), hep-ph/0207004.

[15] V. Ravindran, J. Smith, and W. L. van Neerven, Nucl. Phys. **B665**, 325 (2003), hep-ph/0302135.

[16] S. Catani, D. de Florian, M. Grazzini, and P. Nason, JHEP **07**, 028 (2003), hep-ph/0306211.

[17] S. Moch and A. Vogt, Phys. Lett. **B631**, 48 (2005), hep-ph/0508265.

[18] V. Ravindran, J. Smith, and W. L. van Neerven (2006), hep-ph/0608308.

[19] T. Sjostrand, Phys. Lett. **B157**, 321 (1985).

[20] G. Corcella et al. (2002), hep-ph/0210213.

[21] T. Sjostrand, S. Mrenna, and P. Skands, JHEP **05**, 026 (2006), hep-ph/0603175.

[22] S. Frixione and B. R. Webber, JHEP **06**, 029 (2002), hep-ph/0204244.

[23] S. Frixione, P. Nason, and B. R. Webber, JHEP **08**, 007 (2003), hep-ph/0305252.

[24] J. C. Collins and D. E. Soper, Nucl. Phys. **B193**, 381 (1981).

[25] J. C. Collins and D. E. Soper, Phys. Rev. Lett. **48**, 655 (1982).

[26] J. C. Collins and D. E. Soper, Nucl. Phys. **B197**, 446 (1982).

[27] J. C. Collins, D. E. Soper, and G. Sterman, Nucl. Phys. **B250**, 199 (1985).

[28] C. Balazs and C.-P. Yuan, Phys. Lett. **B478**, 192 (2000), hep-ph/0001103.

[29] E. L. Berger and J.-W. Qiu, Phys. Rev. **D67**, 034026 (2003), hep-ph/0210135.

[30] A. Kulesza, G. Sterman, and W. Vogelsang, Phys. Rev. **D69**, 014012 (2004), hep-ph/0309264.

[31] G. Bozzi, S. Catani, D. de Florian, and M. Grazzini, Phys. Lett. **B564**, 65 (2003), hep-ph/0302104.

[32] G. Bozzi, S. Catani, D. de Florian, and M. Grazzini, Nucl. Phys. **B737**, 73 (2006), hep-ph/0508068.

[33] C. Balazs, J. Huston, and I. Puljak, Phys. Rev. **D63**, 014021 (2001), hep-ph/0002032.

[34] J. Huston, I. Puljak, T. Sjostrand, and E. Thome (2004), hep-ph/0401145.

[35] C. Balazs, M. Grazzini, J. Huston, A. Kulesza, and I. Puljak (2004), hep-ph/0403052.

[36] M. Dobbs et al. (2004), hep-ph/0403100.

[37] ATLAS, Detector and Physics Performance Technical Design Report, Vol.II, CERN/LHCC 99-14/14, and references therein.

[38] CMS, Technical Design Report, Vol.II: Physics Performance, CERN/LHCC 2006-021, and references therein.

[39] V. M. Abazov et al. (D0), Phys. Rev. Lett. **96**, 011801 (2006), hep-ex/0508054.

[40] A. Bredenstein, A. Denner, S. Dittmaier, and M. M. Weber, Phys. Rev. **D74**, 013004 (2006), hep-ph/0604011.

[41] C. M. Carloni Calame et al., Nucl. Phys. Proc. Suppl. **157**, 73 (2006), hep-ph/0604033.

[42] A. Bredenstein, A. Denner, S. Dittmaier, and M. M. Weber (2006), hep-ph/0611234.

[43] C. Balazs and C.-P. Yuan, Phys. Rev. **D56**, 5558 (1997), hep-ph/9704258.

[44] J. C. Collins and D. E. Soper, Phys. Rev. **D16**, 2219 (1977).

[45] F. Wilczek, Phys. Rev. Lett. **39**, 1304 (1977).

[46] J. R. Ellis, M. K. Gaillard, D. V. Nanopoulos, and C. T. Sachrajda, Phys. Lett. **B83**, 339

(1979).

[47] H. M. Georgi, S. L. Glashow, M. E. Machacek, and D. V. Nanopoulos, Phys. Rev. Lett. **40**, 692 (1978).

[48] T. G. Rizzo, Phys. Rev. **D22**, 178 (1980).

[49] LEPEWWG (2003), hep-ex/0312023.

[50] G. Degrassi, P. Gambino, M. Passera, and A. Sirlin, Phys. Lett. **B418**, 209 (1998), hep-ph/9708311.

[51] Q.-H. Cao and C.-P. Yuan, Phys. Rev. Lett. **93**, 042001 (2004), hep-ph/0401026.

[52] J. Pumplin et al., JHEP **07**, 012 (2002), hep-ph/0201195.

[53] R. P. Kauffman, Phys. Rev. **D44**, 1415 (1991).

[54] R. P. Kauffman, Phys. Rev. **D45**, 1512 (1992).

[55] C. P. Yuan, Phys. Lett. **B283**, 395 (1992).

[56] D. de Florian and M. Grazzini, Phys. Rev. Lett. **85**, 4678 (2000), hep-ph/0008152.

[57] D. de Florian and M. Grazzini, Nucl. Phys. **B616**, 247 (2001), hep-ph/0108273.

[58] A. Vogt, S. Moch, and J. A. M. Vermaseren, Nucl. Phys. **B691**, 129 (2004), hep-ph/0404111.

[59] F. Landry, R. Brock, P. M. Nadolsky, and C. P. Yuan, Phys. Rev. **D67**, 073016 (2003), hep-ph/0212159.

[60] M. Dittmar and H. K. Dreiner, Phys. Rev. **D55**, 167 (1997), hep-ph/9608317.

[61] T. Han and R.-J. Zhang, Phys. Rev. Lett. **82**, 25 (1999), hep-ph/9807424.

[62] T. Han, A. S. Turcot, and R.-J. Zhang, Phys. Rev. **D59**, 093001 (1999), hep-ph/9812275.

[63] G. L. Kane and C.-P. Yuan, Phys. Rev. **D40**, 2231 (1989).

[64] V. D. Barger, K. Cheung, A. Djouadi, B. A. Kniehl, and P. M. Zerwas, Phys. Rev. **D49**, 79 (1994), hep-ph/9306270.

[65] V. D. Barger, T. Han, and J. Ohnemus, Phys. Rev. **D37**, 1174 (1988).

[66] C. P. Buszello, I. Fleck, P. Marquard, and J. J. van der Bij, Eur. Phys. J. **C32**, 209 (2004), hep-ph/0212396.

[67] B. Mellado, S. Paganis, W. Quayle, and S. L. Wu (2004), Analysis of H->ZZ->4l at ATLAS, ATL-COM-PHYS-2004-042.

[68] M. Pieri, prepared for Hadron Collider Physics Symposium 2005, Les Diablerets, Switzerland, 4-9 Jul 2005, Searches for Higgs bosons at LHC.